Cement and Concrete Research 81 (2016) 24–37

Contents lists available at ScienceDirect

Cement and Concrete Research

journal homepage: www.elsevier.com/locate/cemconres

Controlling the reaction kinetics of sodium carbonate-activated slag cements using calcined layered double hydroxides

Xinyuan Ke, Susan A. Bernal *, John L. Provis *

Department of Materials Science & Engineering, The University of Sheffield, Sheffield S1 3JD, United Kingdom

ARTICLE INFO

Article history:
Received 29 June 2015
Accepted 27 November 2015
Available online 21 December 2015

Keywords:
Calorimetry (A)
Kinetics (A)
Alkali activated cement (D)
Granulated blast furnace slag (D)
MgO (D)

ABSTRACT

In this study, Na_2CO_3-activated slag cements were produced from four different blast furnace slags, each blended with a calcined layered double hydroxide (CLDH) derived from thermally treated hydrotalcite. The aim was to expedite the reaction kinetics of these cements, which would otherwise react and harden very slowly. The inclusion of CLDH in these Na_2CO_3-activated cements accelerates the reaction, and promotes hardening within 24 h. The MgO content of the slag also defines the reaction kinetics, associated with the formation of hydrotalcite-type LDH as a reaction product. The effectiveness of the CLDH is associated with removal of dissolved CO_3^{2-} from the fresh cement, yielding a significant rise in the pH, and also potential seeding effects. The key factor controlling the reaction kinetics of Na_2CO_3-activated slag cements is the activator functional group, and therefore these cements can be designed to react more rapidly by controlling the slag chemistry and/or including reactive additives.

1. Introduction

Alkali-activated materials derived from an aluminosilicate precursor have become the object of much study in the past two decades, gaining interest as an alternative to traditional Portland cement, and are now produced on an industrial scale and commercialised in several countries [1–3].

However, the performance of alkali-activated slag materials cannot easily be predicted from simple mix design considerations, as there are many additional factors that can modify their microstructure and transport properties, such as the fineness, composition, mineralogy and thermal history of the slag used, the type and concentration of the alkali activator, the mixing time, and the curing conditions [4–7]. Among these, the selection of the type of activator strongly influences the properties of the cement produced, and also the environmental impact associated with its production. The most widely used alkali activators, which are sodium hydroxide and sodium silicate, contribute the majority of the environmental footprint assigned to alkali-activated cements [8,9]. In the search for more cost-effective, user-friendly and environmentally friendly alternatives, the use of near-neutral salts such as sodium carbonate as activators for blast furnace slag has attracted the attention of academia and industry [9–11].

Among the main challenges faced in practice when using sodium carbonate as an activator for slag are the long setting time and delayed compressive strength development which are often observed. Sodium carbonate-activated slag pastes often require a much longer time to set than sodium silicate or hydroxide activated slag pastes, up to 5 days in some cases [10,12–14]. The prolonged hardening process is related to the slow development of the alkalinity required to initiate the dissolution of the slag. In the alkali-activation process, Ca^{2+} released from the dissolved slag must react with CO_3^{2-} from the activator to form carbonate salts such as calcite and gaylussite, to increase the pH through the release of hydroxide ions [10]. This takes place prior to the precipitation of C–(A)–S–H gel, consuming the Ca^{2+} released by the slag, and as the initial pH of the sodium carbonate activator is below 12, the dissolution of silicate species is slow. With surplus CO_3^{2-} ions present in the system, the pH of the liquid phase increases only slowly due to the unfavourable protonation process of the anhydrous slag [10,12]. After the CO_3^{2-} ions have been exhausted, the later stage reaction mechanism is comparable to that of a NaOH-activated slag [10].

Understanding the relationship between the slag chemistry and the kinetics of reaction of sodium carbonate activated slag cements is imperative for selecting a suitable carbonate binding agent to accelerate the reaction of these materials. Systematic studies of the influence of slag chemistry on sodium carbonate-activated slag have not previously been published, but the work which is available for silicate and hydroxide activators shows that the different oxides present in the slag, such as MgO and Al_2O_3, control the kinetics of reaction and the phase assemblage [15–18]. In most studies, where slags with moderate Mg content were used, the Na_2CO_3 activated slag paste required a longer time to set than when using equivalent doses of Na_2SiO_3 or NaOH activator [10,12,14,17,19]. Conversely, Shi et al. [20] used a basic slag with high MgO content (14.6 wt.%), and identified that upon activation with sodium carbonate the samples set within 24 h, which was faster than when

* Corresponding authors. Tel.: +44 114 222 5490.
E-mail addresses: s.bernal@sheffield.ac.uk (S.A. Bernal), j.provis@sheffield.ac.uk (J.L. Provis).

http://dx.doi.org/10.1016/j.cemconres.2015.11.012

using an equivalent dose of sodium silicate activator. This shows that the slag chemistry plays a significant role in defining the kinetics of reaction when using sodium carbonate as alkali activator, and higher MgO content favours a shorter setting time.

The MgO content of slag has also been reported to affect the reaction kinetics, microstructure and strength development of sodium silicate- or hydroxide-activated slag, related to availability of Al and the formation of layered double hydroxides with a hydrotalcite-like structure [4,16,17]. Hydrotalcite-like phases share the general formula $M_x^{2+}M_y^{3+}(OH)_{2x+3y-nz}(A^{n-})_z \cdot mH_2O$, where A^{n-} is often Cl^-, CO_3^{2-} or NO_3^-, and x/y is generally between 2 and 3 [21,22]. The Mg^{2+}–Al^{3+} members of this group are commonly identified in alkali-activated slag systems when the MgO content in the raw material is higher than 5 wt.%, in conjunction with the C–(A)–S–H gel which dominates the binder structure [8]. Hydrotalcite-like phases have also been seen to increase the resistance to carbonation of alkali silicate-activated slag [17]; the high CO_2 uptake capacity and selectivity of these Mg–Al layered double hydroxides make them effective as in-situ carbonate binding agents.

Thermally treated LDHs, also described as calcined layered double hydroxides (CLDH), can re-crystallise to produce LDHs in an aqueous environment, and the chemical composition and structure of CLDH derived from hydrotalcite are related to the nature of the untreated LDH and the thermal activation conditions [23,24]. CLDH has been widely used in the past three decades as an adsorbent for water purification [25,26] and as a catalyst for organic synthesis [27,28]. Recently, hydrotalcite and its modified forms have attracted the attention of the cement industry as additions to increase the amount of LDH phases forming in cements to improve the ionic binding of chlorides, and therefore the durability of steel-reinforced concretes [29,30].

In this study, four commercial slags with different chemical compositions were used to produce Na_2CO_3 activated slag cements. The relationships between slag chemistry and sodium carbonate activation are discussed, covering both kinetics of reaction and phase assemblage evolution. CLDH was added as a carbonate binding agent in the four different Na_2CO_3-activated slag systems, and its effects on the reaction rate, setting time and phase assemblage evolution were evaluated.

2. Experimental programme

2.1. Materials

The chemical compositions of the four slags used in this study are listed in Table 1. The Blaine fineness, and the average particle size d_{50} determined using laser diffraction, of each slag are reported in Table 2. Slag IDs are assigned according to the MgO content of each of the materials.

The activator used in this study was prepared by pre-dissolving commercial sodium carbonate powder (Sigma Aldrich, Na_2CO_3 ≥99.5%) into distilled water.

CLDH was produced by thermally treating a synthetic hydrotalcite (Sigma Aldrich) at 500 °C at a heating rate of 5 °C/min and with a hold time of 3 h, then allowing the material to cool naturally in the furnace to 105 °C before it was moved to a sealed centrifuge tube and kept in a desiccator under vacuum. This prevented the contamination of CLDH by water and CO_2 from the atmosphere.

The MgO and Al_2O_3 contents of the hydrotalcite prior to thermal treatment were determined by XRF, and the C and H contents were determined using a CHNS Analyser (Perkin Elmer 2400), which yielded a charge-balanced chemical composition of $Mg_{0.7}Al_{0.3}(OH)_2(CO_3)_{0.15}\cdot 0.63H_2O$. The thermal treatment conditions adopted in this study were selected based on the experimental results discussed previously by Hibino et al. [24]. The CLDH produced in this study has a chemical composition of $Mg_{0.7}Al_{0.3}O_{1.15}$ [31]. Detailed characterisation of the LDH used in this study, before and after thermal treatment, is reported in the Supporting Information.

Table 1
Chemical composition of anhydrous slags, determined by X-ray fluorescence (XRF). LOI corresponds to the loss on ignition at 1000 °C. All elements are represented on an oxide basis regardless of their oxidation state in the slag.

Slag	CaO	SiO_2	Al_2O_3	MgO	SO_3	Fe_2O_3	TiO_2	MnO	K_2O	Others	LOI
M01	42.9	31.6	14.6	1.2	2.0	1.1	0.4	0.3	0.3	0.2	2.0
M05	42.3	32.3	13.3	5.2	2.9	0.6	0.5	0.2	0.3	0.0	−0.5
M06	41.3	36.0	11.3	6.5	0.7	0.3	0.5	0.3	0.4	0.3	2.0
M14	33.9	37.4	9.0	14.3	0.7	0.4	0.4	1.0	0.5	0.4	1.9

Table 2
Physical properties of the anhydrous blast furnace slags.

Slag	Blaine fineness (cm^2/g)[a]	d_{50} (μm)[b]
M01	4012 ± 49	14.8
M05	4435 ± 109	13.8
M06	5056 ± 22	11.2
M14	4794 ± 44	14.3

[a] Conducted according to ASTM C204-11; quoted uncertainties are the standard deviation of four replicate determinations.
[b] Determined by laser diffraction using a dry dispersion unit, at least 4 measurements were taken for each slag, with standard deviation ±0.1 μm.

2.2. Sample preparation

Sodium carbonate-activated slag pastes with the addition of different amounts of CLDH were produced using each of the slags studied. The formulations of the pastes produced are shown in Table 3. Samples prepared without CLDH addition are referred to as 0 wt.% throughout the paper. Samples prepared with 2 wt.% and 10 wt.% of CLDH (by mass of anhydrous slag) are described as modified samples. For mix design purposes, the CLDH added to these cements was considered as an additive, and the amount of activator and water added to each unit mass of slag was kept constant. All the pastes were cast in centrifuge tubes, then sealed and stored at room temperature (20 ± 3 °C) until testing.

To aid in understanding the effect of addition of CLDH to the activated system, two complementary experiments were carried out as references. Only slag M06 was used in this part of the study.

- For sample Ref-1 (Table 3), synthetic hydrotalcite (Sigma Aldrich) was used instead of CLDH, with the aim of evaluating potential seeding effects related to LDH addition.
- For sample Ref-2, a water to binder (anhydrous slag + anhydrous activator) ratio of 0.35 was used instead of 0.4, and no CLDH was added. The w/b ratio 0.35 was calculated by subtracting the amount of water consumed by CLDH, (see detailed calculations in Supporting Information). This sample was designed with the aim of identifying any changes in the kinetics of reaction due to the water consumed during the re-hydration of the CLDH; this will be discussed in detail in Section 3.6.

The formulations of all of the binders produced are given in Table 3.

2.3. Test methods

For fresh pastes, isothermal calorimetry experiments were conducted using a TAM Air isothermal calorimeter at a base temperature of 25 ± 0.02 °C. The fresh paste was prepared by external hand-mixing for 3 min, weighed into an ampoule, and immediately placed in the calorimeter to record heat flow for the first 300 h of reaction. All results were normalised by the total mass of paste.

Table 3
Formulations of the pastes produced using four different slags.

ID	Slag (g)	Na_2CO_3 (g)	H_2O (g)	Chemical additive (g)	%Na_2CO_3 (wt.%)	pH of activator	w/b[a]
0 wt.%	10	0.8	4.32	None	8.00	11.70	0.40
2 wt.%	10	0.8	4.32	0.2 CLDH	8.00	11.70	0.40
10 wt.%	10	0.8	4.32	1.0 CLDH	8.00	11.70	0.40
Ref-1	10 (M06)	0.8	4.32	1.0 HT	8.00	11.70	0.40
Ref-2	10 (M06)	0.8	3.78	None	8.00	11.89	0.35

[a] w/b = water/binder mass ratio (where binder is defined as slag + mass of sodium carbonate).

Samples cured for 28, 90 and 180 days were crushed and immediately treated with acetone to arrest reaction. The powdered specimens were then dried in a desiccator for 24 h to remove the solvent, and then analysed by:

- X-ray diffraction (XRD), using a Bruker D2 Phaser instrument with Cu-Kα radiation and a nickel filter. The tests were conducted with a step size of 0.02° and a counting time of 3 s/step, from 5° to 55° 2θ.
- Environmental scanning electron microscopy and energy dispersive X-ray spectroscopy (SEM–EDX), using a Hitachi benchtop ESEM TM3030 coupled with a Bruker Quantax 70 X-ray microanalysis detector. An acceleration voltage of 15 kV and a working distance of 1 mm were applied. Polished but uncoated samples were used for both backscattered electron imaging and EDX analysis under charge-up reduction mode. Over 60 points (EDX spots) per sample at each age and formulation were analysed.
- Solid-state ^{27}Al MAS NMR spectra were acquired at 104.20 MHz, on a Varian VNMRS 400 (9.4 T) spectrometer and a probe for 4 mm o.d. zirconia rotors, a spinning speed of 12–14 kHz with a pulse duration of 1 μs (approximately 25°), a relaxation delay of 0.2 s, and a minimum of 7000 repetitions. ^{29}Si MAS NMR spectra were collected at 79.4 MHz on the same spectrometer using a probe for 6.0 mm o.d. zirconia rotors, and a spinning speed of 6 kHz. The ^{29}Si MAS NMR were collected with a 90° pulse duration of 4.5 or 6.4 μs, a relaxation delay of 5 s, and between 6000 and 17000 repetitions. ^{29}Si and ^{27}Al chemical shifts are referenced to external samples of tetramethylsilane (TMS) and a 1.0 M aqueous solution of $Al(NO_3)_3$, respectively.

3. Results and discussion

3.1. Kinetics of reaction

Fig. 1 shows the heat flow from the four different slags studied, during activation with a sodium carbonate solution (Table 3), with addition of 0, 2 and 10 wt.% of CLDH. In all samples it is observed that the reaction takes place in two stages. The first occurs within the first 10 h of reaction (insets on each part of Fig. 1), except for the case of the lowest-MgO slag (M01), where a low heat release was detected due to the low level of precipitation of reaction products in the first hours of reaction. The first stage of the reaction is followed by a dormant or induction period, where a very low rate of heat release was detected. The duration of the pre-induction period is strongly dependent on the slag composition and the level of CLDH addition. In the second stage of heat release, the nucleation, growth and precipitation of a large amount of reaction products take place, which is associated with a high heat release. This takes place between 25 h and 300 h after the start of the reaction, depending on the slag composition and the addition of CLDH. Samples prepared without CLDH addition show a very long delay in the appearance of this peak, consistent with the known slow setting of Na_2CO_3-activated slag binders, although the MgO content of the slag is seen to have a significant influence on the time at which this peak appears.

In the first stage of the reaction, a pre-induction band composed of two distinctive peaks was observed in all the samples, except for slag M01. The pre-induction peaks are associated with the formation of calcite and gaylussite, which have been reported as the initial reaction products forming in Na_2CO_3-activated slag binders [10,12]. As slag dissolution progresses, even at low rates within the first hours of reaction, the formation of the reaction product phases such as calcium silicate hydrates (C–S–H) and secondary aluminate-containing reaction products has been observed [10,12–14], corresponding to the second peak identified within the pre-induction period (insets of each part of Fig. 1).

For the slag M01 in the absence of CLDH, the initial precipitation of reaction products was observed after 25.7 h, and the peak was low and broad. The slowly evolving pre-induction period was followed by a prolonged dormant period that lasted for 90.1 h before the acceleration period started. The acceleration and deceleration periods evolved slowly, with the slowest rate of acceleration among all of the samples studied. The addition of 2 wt.% and 10 wt.% CLDH shortened the dormant period to 32.0 h and 6.7 h (Table 4), respectively, and the onset time of the acceleration period was thus shifted significantly earlier. The heat flow curve during the acceleration–deceleration period became less broad and more intense with the increasing addition of CLDH.

The activated slag M05 paste without CLDH addition (Fig. 1B) also presented a prolonged induction period; however, a secondary peak associated with precipitation of reaction products was identified in the pre-induction period after 3.2 h of reaction (Table 4). The acceleration period started after 151 h, and showed a much steeper acceleration than the slag M01, indicating that the growth of reaction products was much more rapid in the higher-MgO system once nucleation did take place. The deceleration period then evolved slowly, but showed two distinct humps that are likely to be indicating the precipitation of different types of reaction products at different times. With 2 wt.% CLDH addition, the induction period was shortened to 15.3 h, and the acceleration period started after 36.5 h of activation, with the double-peak structure of the acceleration–deceleration period again notable. When the CLDH addition was increased to 10 wt.%, all the stages of the reaction occurred within the first 24 h after mixing. A negligible induction period was observed for this cement, and a single narrow peak with a rapid acceleration up to a maximum heat evolution at 18 h was identified. In the pre-induction period (insert Fig. 1B), it is notable that the intensity of the secondary peak increased with the addition of higher contents of CLDH in the sample, and in the case of 10 wt.% of CLDH addition, the peak shifted towards shorter times of reaction.

For Na_2CO_3 activated M06 (Fig. 1C) and M14 (Fig. 1D) slags, the CLDH addition has a similar effect in modifying the kinetics of reaction of these cements, to the observations for M01 and M05 based pastes. The M06 and M14 activated slags without CLDH addition react significantly faster than samples prepared with slags M01 and M05 (Fig. 1A, B and Table 4), indicating that the slag chemistry has a significant effect on the kinetics of reaction of Na_2CO_3-activated cements. Each of the stages of the reaction processes becomes significantly more rapid with CLDH addition, and the peak heat evolution rates of both the pre-induction and the acceleration/deceleration peaks are consistently increased. In contrast to the observations for Na_2CO_3-activated M01 and

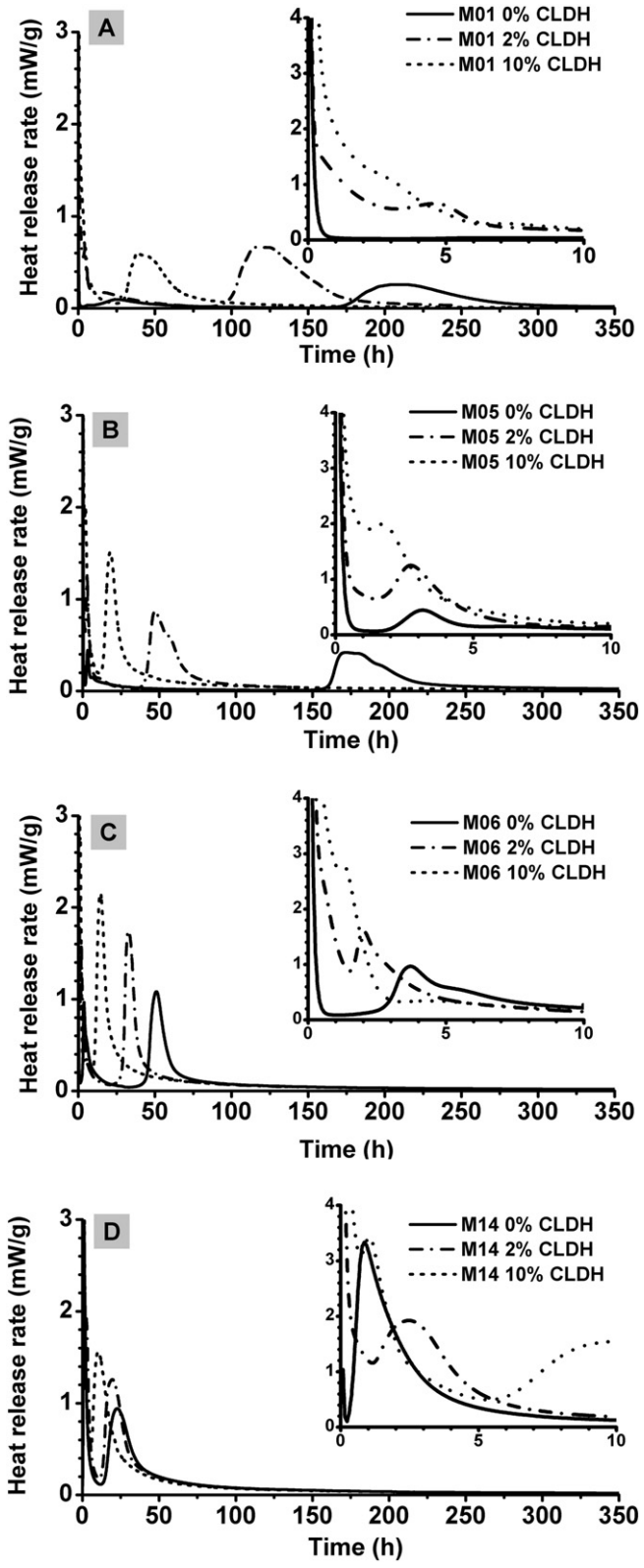

Fig. 1. Isothermal calorimetry data for Na_2CO_3-activated slag cements, produced with slags (A) M01, (B) M05, (C) M06 and (D) M14, as a function of the percentage of CLDH addition. All curves are normalised by the total mass of paste tested.

M05 slags, a much shorter dormant period is observed when using M06 and M14, with and without CLDH addition, and consequently the main peak is identified within the first 24 h of reaction for each of these slags. This suggests that the precipitation of the different reaction products forming when using high MgO content slags (>6 wt.%) is not significantly delayed when using a Na_2CO_3 solution as sole alkali activator, unlike the situation for lower-MgO slags.

3.2. X-ray diffraction (XRD)

3.2.1. Effects of slag chemistry and addition of CLDH on the phase assemblage of Na_2CO_3-activated cements

The X-ray diffraction patterns of the sodium activated slag cements after 28 days of reaction (Fig. 2) show the formation of three types of crystalline phases in all the cements assessed: carbonates, LDHs and tobermorite-like C–(A)–S–H gels, whose composition and features are strongly dependent on the slag chemistry and CLDH content.

Gaylussite ($Na_2Ca(CO_3)_2 \cdot 5H_2O$, PDF #00-021-0343) and calcite (PDF #01-086-0174) were the major carbonates identified in all samples, independent of the slag composition and the content of CLDH. The intensities of the gaylussite reflections are similar in all the 0 wt.% CLDH pastes after 28 days of curing. In samples modified by 2 wt.% CLDH, the intensities of the peaks assigned to gaylussite decrease compared to the 0 wt.% formulations, and this phase could barely be identified in the 10 wt.% CLDH modified samples. Additional metastable polymorphs of calcium carbonate including vaterite ($CaCO_3$, PDF #01-072-0506) and aragonite ($CaCO_3$, PDF #00-041-1475) were also observed in most slag pastes. The reflections assigned to calcite, vaterite and aragonite remained almost unchanged in the CLDH modified samples compared to the respective 0 wt.% samples. It is notable that higher intensity reflections of gaylussite are observed (Fig. 2.D) in the specimens produced with the slag (M14) with higher MgO content and the higher CLDH addition. The observation here might indicate the limited phase modification capacity of CLDH in MgO-rich slag cements.

Two types of LDH phases were identified in the Na_2CO_3 activated 0 wt.% samples: calcium hemicarboaluminate ($C_4A\underline{c}_{0.5}H_{12}$, PDF #00-036-0129), which is a member of the 'AFm' (hydrocalumite-like) group and known in cement chemistry as 'hemicarbonate', and a hydrotalcite-like phase ($Mg_4Al_2(OH)_{12}CO_3 \cdot 3H_2O$, PDF #00-014-0525). The relative concentrations of these two types of LDH phase in each sample are directly related to the chemical composition of the slags, and the dose of CLDH added. A higher content of MgO in the slag precursor favoured the formation of Mg–Al type LDH phases to consume aluminium. However, with low MgO content but high Al_2O_3 content, there is not sufficient MgO to consume the excess aluminium, and therefore the hemicarbonate phase may form [32,33]. Thus, in the paste with the lowest MgO content (Fig. 2A, M01_0% CLDH), this was the only LDH phase identified. In the slags with moderate MgO content, M05 and M06, both types of LDH phases were present after 28 days of curing. When the anhydrous slag precursor contains a high MgO content, as in the case of M14, only the Mg–Al type of LDH (the hydrotalcite-like phase) was identified. The same trends are observed in the samples modified by 2 wt.% and 10 wt.% of CLDH, along with an increase in the content of the hydrotalcite-like phase in all the CLDH modified samples attributed to the recrystallisation of the CLDH [34–36]. However, the hydrotalcite-like phase derived from the recrystallisation of the CLDH cannot be distinguished by XRD from the additional hydrotalcite-like phase forming through activation of the slags.

It is worth noting that hemicarbonate has not been widely reported as a reaction product in sodium silicate-activated slag systems, but has been observed in Portland cement/slag blended systems when the Al_2O_3 content in slag is high and calcite is present in the system, as such conditions favour the formation of AFm type phases, and the presence of carbonate stabilises the hemicarbonate member of this family [32,33,37–39]. A mixture of AFm and hydrotalcite-like phase has also been identified in NaOH-activated slag pastes cured for up to 15 months [40,41]. The formation of mixed LDH phases in sodium carbonate-activated slag might have followed the same mechanism, as the reaction

Table 4
Summary of the heat release curves shown in Fig. 1.

Slag	CLDH addition (wt. %)	Pre-induction period (h)		Duration of induction period (h)[a]	Acceleration–deceleration period		Total heat release (J/g)[b]
		Peak time (h)	Duration (h)[a]		Onset time (h)[a]	Peak time (h)	
M01	0	25.7	74.9	90.1	165.0	210	87.8
	2	4.6	56.3	32.0	88.3	120	172
	10	2.7	20.7	6.7	27.4	43.2	128
M05	0	3.2	62.2	79.6	151.4	170	98.2
	2	2.7	15.3	15.3	36.5	46.7	104
	10	1.7	2.1	2.1	11.4	17.6	142
M06	0	3.7	30.4	30.4	40.3	50.6	102
	2	2.0	14.7	14.7	24.3	33.1	119
	10	1.3	0.7	0.7	9.1	14.0	158
M14	0	0.87	2.48	2.48	13.0	22.3	135
	2	2.5	1.21	1.21	11.5	19.0	142
	10	1.1	0.42	0.42	5.56	10.8	189

[a] The duration of the induction period is determined using the first derivative of its heat flow rate. The start of the induction period (and correspondingly the end of the pre-induction period) is defined as when its first derivative increased from a negative value to greater than -5×10^{-5} mW/g · h. The end of the induction period is identified when its first derivative started to increase above 5×10^{-5} mW/g · h. The first derivative during the induction period is within the range $0 \pm 5 \times 10^{-5}$ mW/g · h.
[b] The total heat release here is the integrated reaction heat, from the start of the reaction to the long-term period where the heat flow is lower than 30 μW/g. The results were normalised by the mass of the paste.

mechanism becomes comparable to NaOH-activation of the slag once the CO_3^{2-} is exhausted [10].

The C–(A)–S–H phases identified in all the samples are close to an aluminium substituted tobermorite-like phase ($Ca_5Si_5Al(OH)O_{17} \cdot 5H_2O$, PDF #00-019-0052; tobermorite-14 Å, PDF #00-029-0331) [42]. The C–(A)–S–H phases formed in each of the slag systems cannot be distinguished solely via XRD, due to the poorly crystalline nature of this reaction product. However, the presence of a broad hump at around 6.4° 2θ in the sample M06_2% CLDH (Fig. 2C), and the disappearance of the high intensity hump at 7.1° 2θ in the sample M14_10% CLDH (Fig. 2D), suggest changes in either the composition or the structure of the C–(A)–S–H phase. This will be further assessed in the following sections via scanning electron microscopy and solid-state nuclear magnetic resonance spectroscopy.

3.2.2. Phase evolution over the time of curing

All of the main crystalline phases identified in the Na_2CO_3-activated slag cement, being gaylussite, LDH phases and C–(A)–S–H gel, present

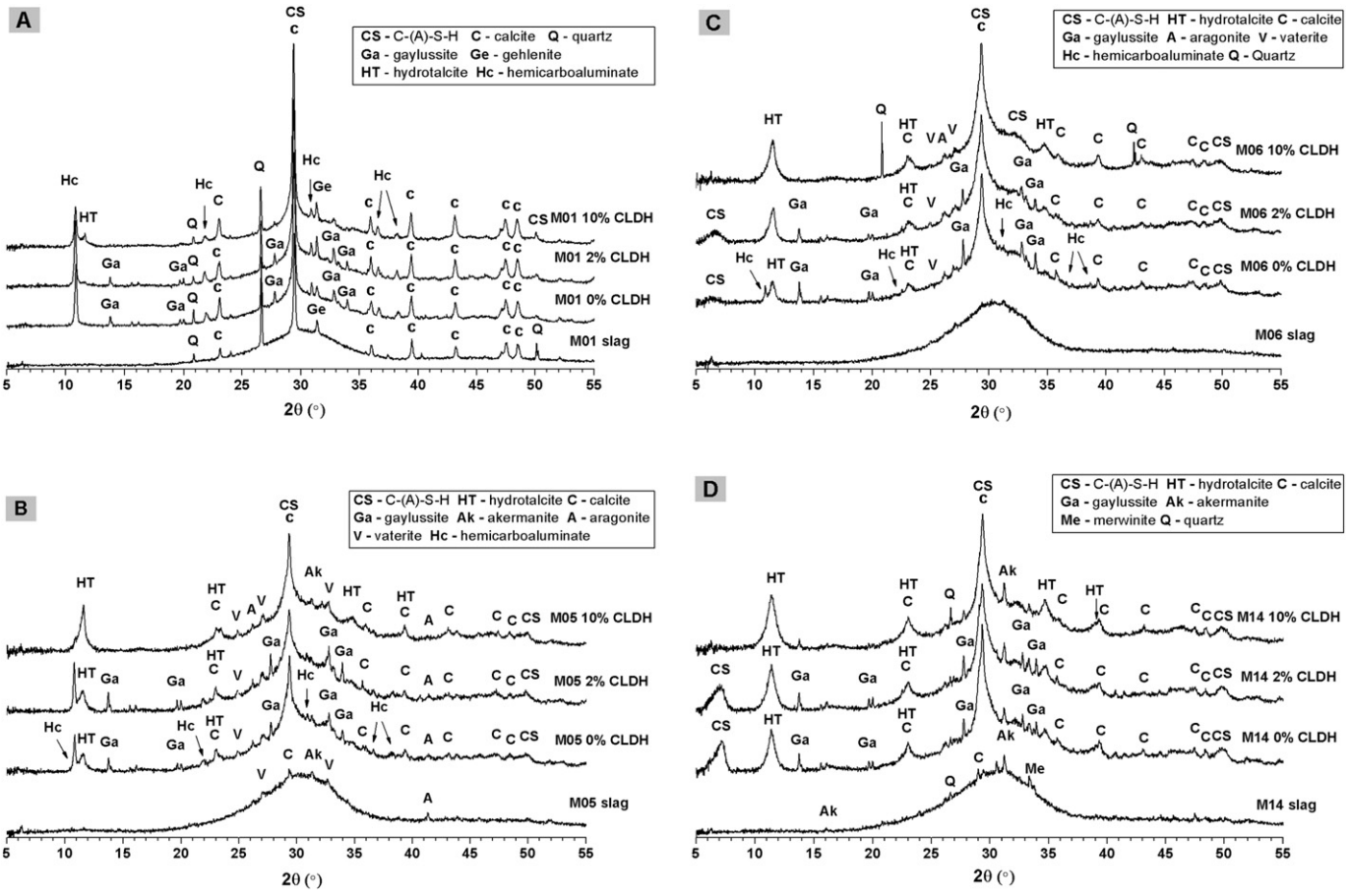

Fig. 2. X-ray diffraction patterns of 28 day-cured sodium carbonate activated slag cements produced with slags: (A) M01, (B) M05, (C) M06, and (D) M14, with 0, 2 and 10 wt.% of CLDH added as marked. Data for each anhydrous slag are also shown in the plots.

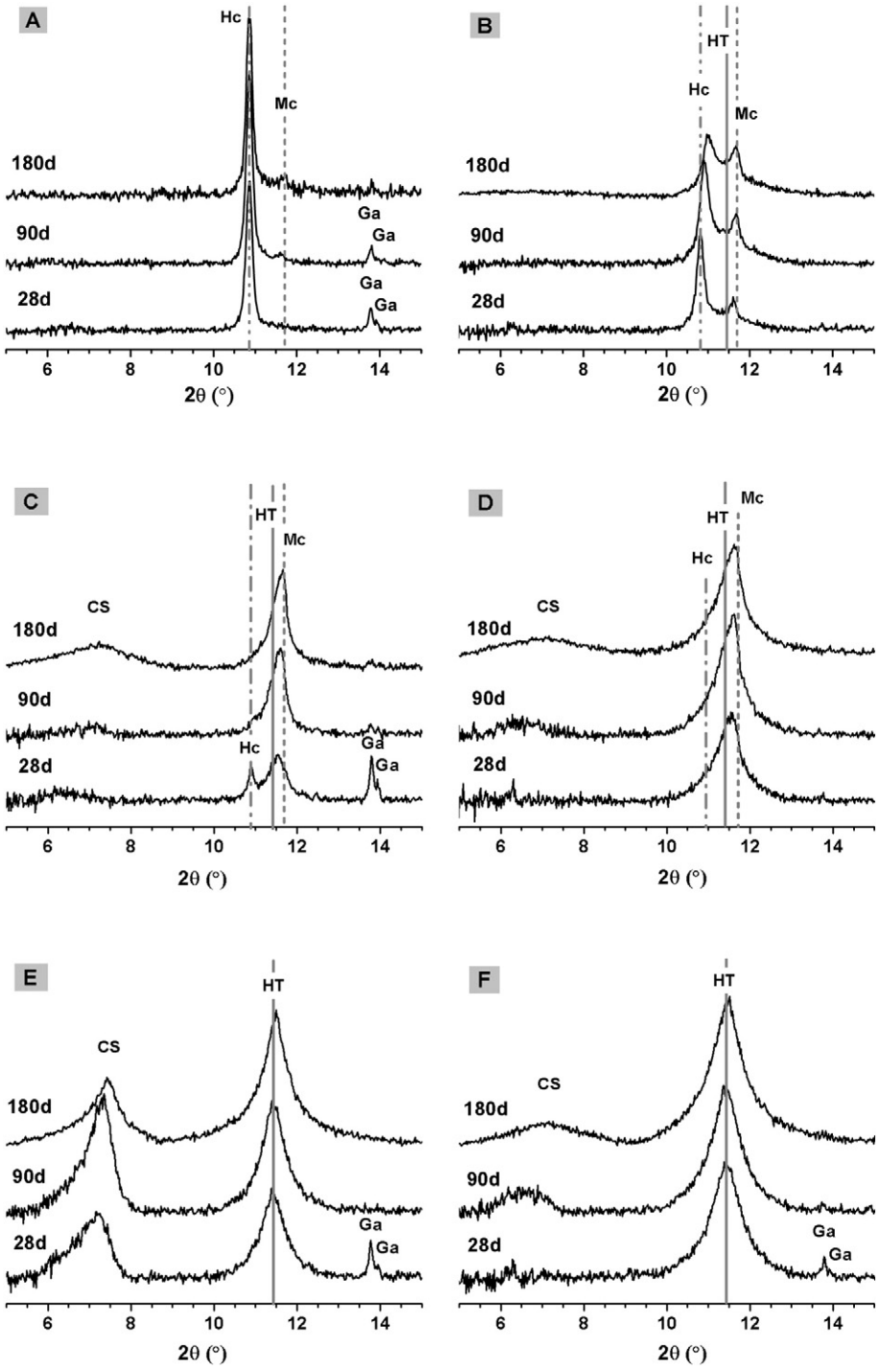

Fig. 3. X-ray diffraction patterns of Na_2CO_3 activated slag M01 with (A) 0 wt.% and (B) 10 wt.% CLDH; slag M06 with (C) 0 wt.% and (D) 10 wt.% CLDH; and slag M14 with (E) 0 wt.% and (F) 10 wt.% CLDH, as a function of the time of curing. Phases marked are: HT — hydrotalcite-like, Hc — hemicarbonate, Mc — monocarbonate, Ga — gaylussite, and CS — C–(A)–S–H.

major diffraction peaks between 5° and 15° 2θ. For a clear and direct comparison across all the samples over the time of curing, XRD patterns in this angular range are presented in Fig. 3 as a function of sample age.

It can be seen (Fig. 3) that gaylussite disappeared from all samples over the time of curing, and it is present only in very small quantities in the M1, M05 and M06 samples containing CLDH. Gaylussite is a transient phase in sodium carbonate activated slag cement, and its consumption is associated with the formation of more stable carbonates. This will be discussed in detail in Section 3.6. The hemicarbonate phase identified in the activated M01 slag with (Fig. 3B) and without (Fig. 3A) CLDH addition decreased over time, and the calcium monocarboaluminate ($C_4\underline{A}c\underline{H}_{11}$, PDF#00-036-0377, 'monocarbonate') phase starts to form [33,39,43,44], predicted to be the stable AFm product in thermodynamic modelling of slag activation by Na_2CO_3 [45]. In Fig. 3B, the basal reflection peak of hemicarbonate shifted towards higher angle, and became wider over time of curing, as a result of partial replacement of OH^- by CO_3^{2-} in hemicarbonate and the consequent formation of a poorly crystalline AFm-(OH^-,CO_3^{2-}) solid solution. The basal reflection peak of monocarbonate is around 11.7° 2θ, which in some cases might overlap with that of the hydrotalcite-like phase, 11.2–11.6° 2θ (marked at 11.4° in Fig. 3). However, in the M01-0% CLDH system (Fig. 3A), the formation of monocarbonate is clearly

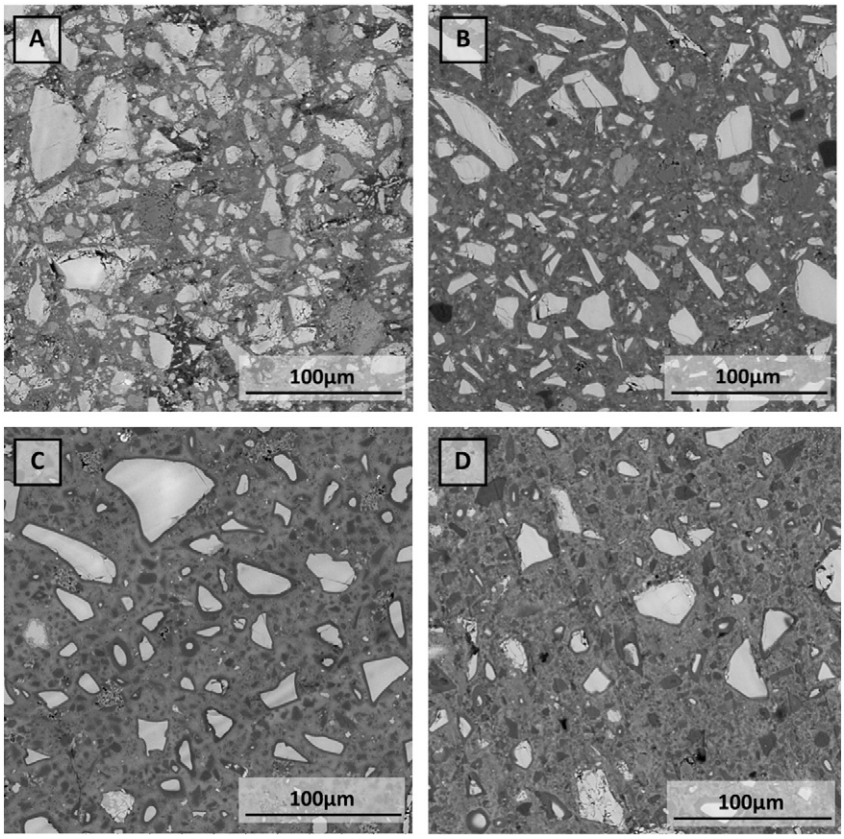

Fig. 4. BSE images of pastes cured for 180 days: slag M01 with (A) 0 wt.% and (B) 10 wt.% CLDH; and slag M14 with (C) 0 wt.% and (D) 10 wt.% CLDH.

identifiable, as no hydrotalcite-like phase is forming. In samples with moderate MgO content (Fig. 3C, E), monocarbonate could not be distinguished via distinct reflection peaks, but the broad peak centred at around 11.4° 2θ shows an asymmetric increase in intensity over time. This increasing asymmetry suggests the formation of a component peak at around 11.7° 2θ, most likely due to monocarbonate. Samples prepared using the high MgO slag M14 do not show reflections indicative of the formation of AFm phases, and thus the peak at around 11.4° 2θ for this formulation, whose intensity increases over the time of curing, is solely assigned to a hydrotalcite-like phase.

Similar trends are identified in the CLDH modified samples, where the high intensity peak of hydrotalcite overlaps with those assigned to hemicarbonate and monocarbonate, obstructing their clear identification. Negligible structural changes are identified in the reaction products of the slag with intermediate content of MgO (Fig. 3D) with the addition of CLDH. In the activated M14 samples with CLDH addition (Fig. 3F), changes in the LDH phase were almost identical to those observed without CLDH addition (Fig. 3E). However, the addition of CLDH seems to modify the structure of the C–A–S–H forming in these systems. This will be further evaluated in the following sections.

In sodium carbonate activated slag systems, hemicarbonate is formed at earlier age (i.e. during the first 28 days) when using slags with medium to low MgO content (M01, M05 and M06). The formation of hemicarbonate is reduced when a higher content of MgO is present, where a higher content of hydrotalcite-like phases is instead formed. In cements based on the high-MgO slag (M14), only the hydrotalcite-like phase was identified. The addition of CLDH increases the formation of hydrotalcite-like phases, and seems also to accelerate the transformation from hemicarbonate to monocarbonate.

In the sodium carbonate activated slag system, the free carbonate ion content in the aqueous phase is reduced as the reaction evolves. Although the formation of monocarbonate from hemicarbonate under such circumstances seems unlikely as the conversion requires additional carbonate, the experimental results suggest that the previously carbonated hydrotalcite-like phase might be able to supply this carbonate. This is in line with recent thermodynamic modelling results for sodium carbonate activated slag, which revealed that monocarbonate is a thermodynamically stable phase in this system, together with a non-carbonated hydrotalcite-like phase [45]. The transformation between these two phases could also be associated with the availability of additional carbonate due to the reaction of precipitated $CaCO_3$, which drives the equilibrium towards the monocarbonate phase [33,44,46].

As seen in Fig. 3, the positions of the basal reflection peaks of the hydrotalcite-like phase vary slightly in different samples with different ages. The basal reflection peak reflects the composition of the mixed metal oxide/hydroxide sheets, the type of interlayer species and the amount of chemically bound water [47,48]. The shifts observed here could be caused either by formation of HT-(OH^-,CO_3^{2-}) solid solutions, or changes in the Mg/Al ratio, as more Al incorporation into a hydrotalcite-like phase leads to a decrease in the angle at which its basal reflection peak is observed [47].

3.3. Scanning electron microscopy

Fig. 4 shows backscattered electron (BSE) images of sodium carbonate activated slag pastes without and with 10 wt.% CLDH, after 180 days of curing. The light grey particles in the micrographs correspond to the unreacted slag particles remaining in the samples, while the grey regions between the remnant slag particles correspond to the main binding phase, consisting mainly of C–(A)–S–H gel and additional reaction product phases such as LDHs and carbonates, as identified by XRD (Figs. 2 and 3). Regions darker in greyscale intensity than the general matrix, which were more numerous and clearly identifiable in moderate to high MgO activated slags (M06 (not shown) and M14) than in samples produced with slags with low MgO content (M01) samples, correspond to fully reacted slag grains and inner reaction product rims

rich in Mg (with the hydrotalcite as a dominant phase) [49,50]. In Fig. 4A, irregular dark grey areas are identified between the slag grains. These are most likely to be sodium–calcium carbonate phases (e.g. gaylussite), as similar features with a chemical composition comparable to that double salt have been observed in sodium carbonate/silicate activated slag cements [11], and the dark greyscale values are consistent with the low mean elemental number of hydrous carbonates.

Fig. 5 shows atomic ratio correlation plots generated from EDX spot analyses of the samples prepared using different slags with 0 wt.% and 10 wt.% of CLDH addition. The spots taken from outer reaction products are referred to as the general matrix in Table 5, excluding large recrystallised hydrotalcite clusters that were not well dispersed during the mixing of the paste. Inner product EDX spots were only taken from slag M14, where clear inner rims were identified. The data presented here show the atomic ratios of the reaction product between the slag grains, which consists of C–(A)–S–H gel and intermixed LDHs. The dashed lines in Fig. 5 showing the ratios Mg/Al = 2 and Ca/Al = 2 are given to clarify the existence of hydrotalcite-like phases and AFm phases [32]. Data points with Al/Si ratios below 0.8 (shown) were chosen for investigation of the chemical composition of the hydrotalcite-like phase and C–(A)–S–H gel, to rule out any interference from well-crystallised AFm phases.

Without the addition of CLDH, the MgO content as well as the Al_2O_3 content controls the chemistry of LDH phases formed as reaction products. With the highest Al_2O_3 content and very low MgO content, slag M01 formed a significant amount of AFm phases to consume excess Al. In slag M06, which has slightly lower Al_2O_3 content but much higher MgO content, the hydrotalcite-like phase was identified as the main LDH with traces of intermixed AFm phases, consistent with the XRD data presented above. This shows that in the presence of MgO, the excess Al in the system is more likely to form hydrotalcite-like phases than AFm phases, consistent with the fact that no AFm phase was identified in samples prepared using slag M14. However, the absence of AFm phases in samples based on slag M14 could also be related to the fact that it contains the lowest Al_2O_3 content and the highest MgO content. The additional CLDH contributed to the increased formation of hydrotalcite-like phase in samples based on all three slags. It also reduced the crystallinity of the AFm phases formed through the reaction of slags M01 and M06, by forming disordered intermixed LDH phases. This corresponds to the XRD results shown in Fig. 3.

The Al/Si ratio of the C–(A)–S–H gel in each alkali-activated slag sample was calculated using the method of Ben Haha et al. [16], Table 5. These values demonstrate a close relationship between the Al_2O_3 content of the slag and the Al/Si ratio in C–(A)–S–H gel, where a

Table 5
Average atomic ratios (Ca/Si and Mg/Al) of Na_2CO_3-activated slag pastes cured for 180 days, using data points shown in the inset plots in Fig. 5 (where Al/Si < 0.8), obtained using EDX analyses of 60 spots per sample (uncertainty in each reported value ±0.02).

Slag		0 wt.% CDLH			10 wt.% CDLH		
		Ca/Si	Al/Si	Mg/Al[a]	Ca/Si	Al/Si	Mg/Al[a]
M01	General matrix	1.22	<0.33	–[b]	1.26	<0.33	1.91
M06	General matrix	1.20	0.20	1.61	1.26	0.21	2.04
M14	General matrix	1.05	0.06	2.09	1.04	0.06	2.16
M14	Inner rim	0.86	0.02	1.86	0.92	0.01	1.84

[a] Mg/Al value is the slope of the line of best fit in a plot of Mg/Al vs Al/Si ratios.
[b] The Mg/Al ratio of the sample M01_0wt.% could not be determined due to the low content of MgO in the anhydrous slag.

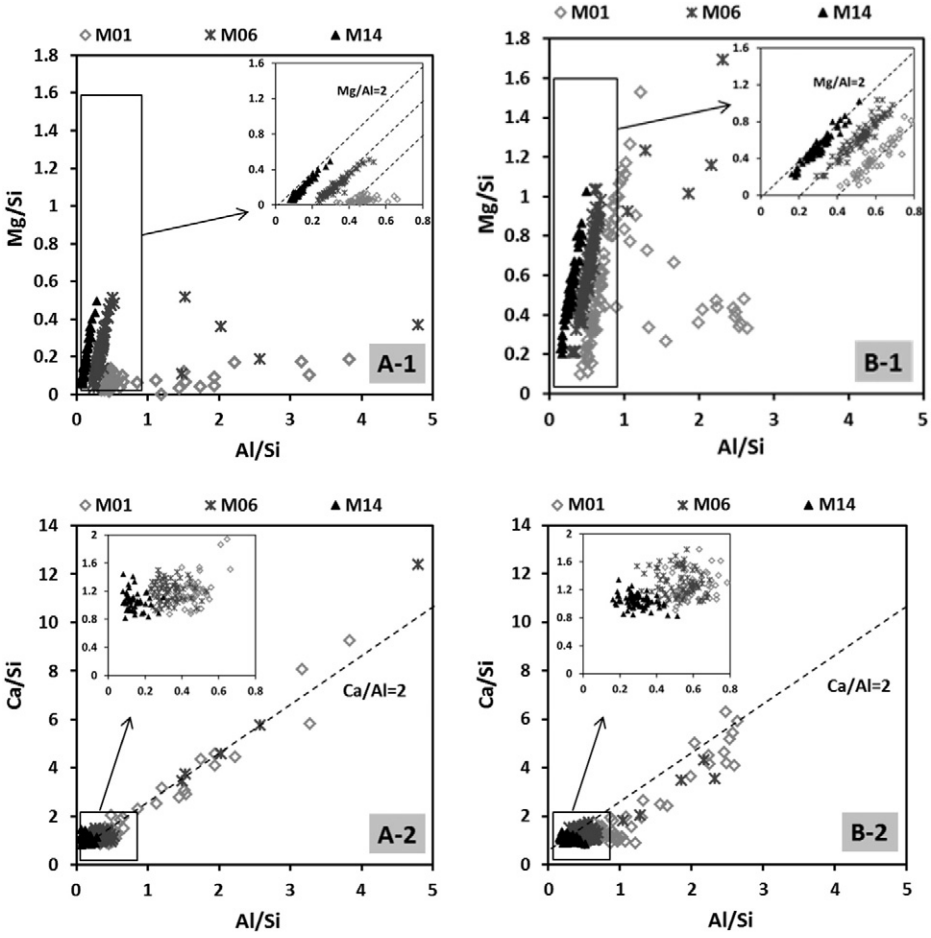

Fig. 5. Atomic ratios calculated from EDX data for Na_2CO_3 activated samples with 0 wt.% (A-1 and A-2) and 10 wt.% (B-1 and B-2) CLDH addition, all after 180 days of curing. (A-1) and (B-1) plotted as Mg/Si vs Al/Si and (A-2) and (B-2) plotted as Ca/Si vs Al/Si.

higher bulk Al_2O_3 content results in a higher Al/Si ratio in the C–(A)–S–H gel (0.2 in slag M06 and 0.06 in slag M14, all with 0 wt.% CLDH addition). The Al/Si ratio of slag M01 calculated using the same method was higher than the maximum possible degree of Al substitution in C–(A)–S–H, due to the presence of intimately intermixed AFm and/or N–A–S–H phases [51,52]. The Al_2O_3 content of the slag controls the degree to which aluminium is able to dissolve and be made available for through-solution reaction processes, and thus defines the Al/Si ratio in C–(A)–S–H gel [51]. This would also explain the observation that in 10 wt.% CLDH modified samples, the Al/Si ratio calculated by this method is slightly higher than that of the samples without CLDH. The recrystallisation of CLDH into hydrotalcite-like phases leads to an increase in pH (see Supporting Information), favouring the dissolution of aluminium and thus resulting in a higher Al/Si ratio.

The Ca/Si ratio in the C–(A)–S–H gel did not change significantly with changes in slag chemistry, with all data points for all samples falling between ratios of 0.8 and 1.6. Those values are higher than the Ca/Si ratios identified in sodium hydroxide-activated or sodium silicate-activated slag cements where slags with similar chemical compositions were used [15–17]. This may be related to the lower alkalinity of the sodium carbonate activator, which brings a lower capacity to dissolve silicate species from the slag grains [53]. However, no systematic change in Ca/Si ratio was observed in the CLDH modified samples compared to the unmodified cements.

The chemical compositions of the inner and outer products of samples prepared using slag M14 were analysed separately using EDX (shown also in Table 5). The Ca/Si ratio of the inner product is distinctly lower than that of the outer product, suggesting that there might be other Ca containing phases forming in the outer product. This is also likely to be caused by the existence of intermixed N–A–S–H gel in the inner product [8,45].

To obtain further insight into the chemistry and structure of the C–(A)–S–H gel in sodium carbonate activated slag cement, analysis by solid-state NMR is required, and is presented below.

3.4. ^{29}Si and ^{27}Al MAS NMR

The ^{29}Si MAS NMR spectra of the anhydrous slags shown in Fig. 6 are in good agreement with the literature for a melilite-type glass [54,55]. For the sodium carbonate activated paste samples, three distinct bands at −79 ppm, −82 ppm and −85 ppm were identified in the main region of the ^{29}Si MAS NMR spectra, which are assigned to a Q^1 site (denoted Q^1(II) for consistency with reference [52]), Q^2(1Al) and Q^2, respectively [55–57]. The residual signal downfield of the −79 ppm band is assigned to Q^0 and Q^1(I) sites [52]. The low intensity, but non-zero, component of the signal which lies upfield of −85 ppm is composed of two bands centred at −88 ppm and −92 ppm respectively, and assigned to highly crosslinked Si sites [58]. The bands in these two positions could be assigned to either Q^4(4Al) and Q^4(3Al) sites in N–A–S–H gel, and/or Q^3(1Al) and Q^3 sites in C–(A)–S–H gel, according to the findings reported by Myers et al. [52] for sodium metasilicate activated slag cements.

Table 6 shows the results of deconvolution of the ^{29}Si MAS NMR spectra using Gaussian curve fitting (exemplified in Fig. 7). For consistency, the deconvolutions were conducted assuming that the anhydrous slag was dissolving congruently, as in sodium silicate or sodium hydroxide activation [15,17,59]. This is generally correct when dissolving calcium aluminosilicate glasses in solutions at a pH above 12.5 [53]. The initial pH of the sodium carbonate activator used in this study was 11.7, which is expected to increase once the CO_3^{2-} in the pore solution is exhausted, either by formation of solid carbonate phases or removal by reaction with the CLDH additive. Therefore, incongruent dissolution of the slag might occur in the early stage of reaction, but it is not expected as the activation reaction progresses, and as the chemistry becomes more comparable to that of NaOH-activation of slag as discussed

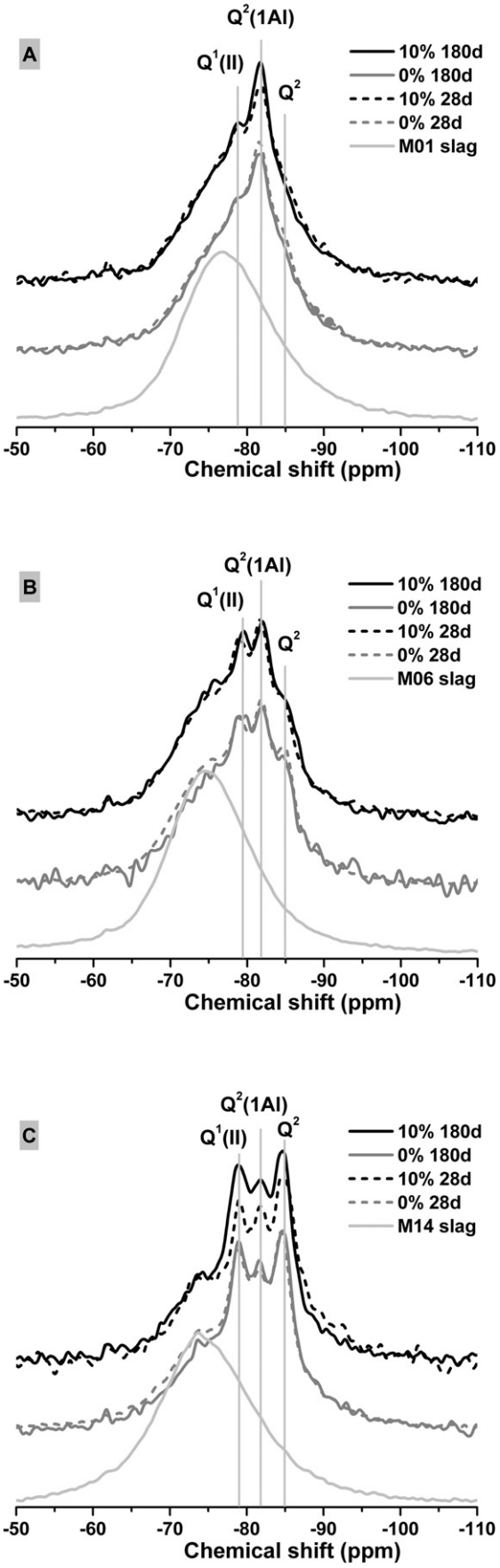

Fig. 6. ^{29}Si MAS NMR spectra of slag pastes prepared using slag M01, M06 and M14.

Table 6
Deconvolution results for ^{29}Si MAS NMR spectra of the sodium carbonate activated slag pastes. Estimated uncertainty in absolute site percentages is ±2%.

	Samples	Total unreacted slag (%)[a]	Reaction products						
			Q^0	Q^1(I)	Q^1(II)	Q^2(1Al)	Q^2	Q^3(1Al) /Q^4(4Al)	Q^3/Q^4(3Al)
			−74 ppm	−76 ppm	−79 ppm	−82 ppm	−85 ppm	−88 ppm	−92 ppm
M01	0% 28 d	64	0	2	7	12	10	2	2
	0% 180 d	64	0	3	5	14	9	3	2
	10% 28 d	64	0	3	5	14	7	4	3
	10% 180 d	62	0	3	6	16	7	3	3
M06	0% 28 d	54	3	1	11	13	12	3	3
	0% 180 d	50	3	2	15	13	11	4	3
	10% 28 d	49	5	1	14	14	10	3	3
	10% 180 d	48	6	2	14	12	12	3	3
M14	0% 28 d	41	4	2	14	12	17	8	4
	0% 180 d	37	3	3	14	13	18	9	4
	10% 28 d	32	5	3	12	14	16	12	6
	10% 180 d	30	6	1	20	15	17	7	3

[a] The actual total unreacted slag (%) might be higher than the calculated value shown here if the dissolution of the glassy slag is incongruent, but this cannot be accurately determined in the absence of a reliable method for the selective dissolution of reaction products in these alkali-activated binder systems.

above. Nonetheless, this must be considered as a potential source of error.

From Table 6, it is evident that a higher extent of slag reaction (as observed by the lower residual slag fraction and much higher C–A–S–H reaction product content) has been reached in mixes based on slags with higher MgO content and lower Al_2O_3 content. Both MgO content and Al_2O_3 content play important roles in defining the intrinsic reactivity of the slag glass, and this is also influenced by the formation of LDH phases which remove the dissolved Mg and Al from solution and provide a further driving force for glass dissolution. This is supported by the fact that the addition of 10 wt.% CLDH is seen to increase the total extent of slag reaction up to 180 days of curing, compared with samples with 0 wt.% CLDH based on the same slags. This shows that the influence of the CLDH is not simply a kinetic effect which accelerates the reaction at early age (as observed by calorimetry); the fact that the CLDH addition induces a higher extent of reaction even up to 180 days indicates that its seeding effect which enhances nucleation and growth of hydrotalcite-group phases is additionally important in defining binder chemistry in the long term.

However, comparing the line shapes of the ^{29}Si MAS NMR spectra of slag pastes prepared using different slags with and without CLDH addition, it is clear that the structure and composition of C–(A)–S–H gel are dominated by effects related to the slag chemistry over the effects of CLDH addition. The intensities of the Q^1(II) and Q^2 sites were higher in pastes prepared using the slag with the highest MgO content (M14), while the intensities of the Q^2(1Al) sites decreased. The increased intensity of Q^1(II) suggests an increase in the content of chain-end sites charge balanced by strongly positively charged cations (e.g. Ca^{2+}) [52], while the increased intensity of Q^2 sites suggests a higher mean chain length. The decrease in the intensities of Q^2(1Al) sites, associated with reduced Al uptake by the C–(A)–S–H gel, is due to the lower Al_2O_3 contents in slags M06 and M14 compared with slag M01, and also the formation of a higher content of LDH phases which consume Al, corresponding to the results of EDX analysis.

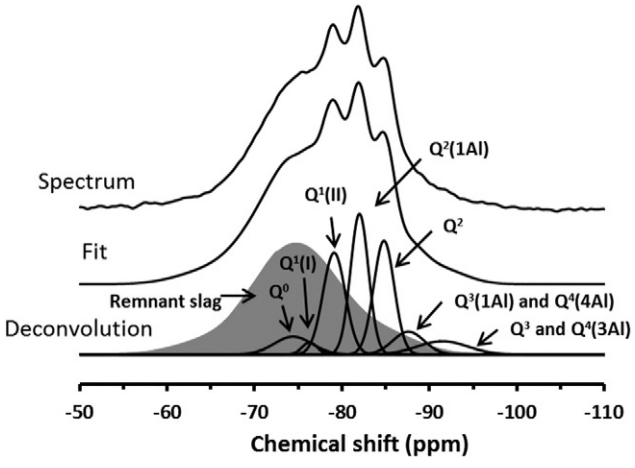

Fig. 7. Deconvoluted ^{29}Si MAS NMR spectrum of slag M06_0% CLDH cured for 28 days. The dark grey band represents the contribution of the remnant slag, which is directly scaled from the spectrum collected for the unreacted slag using the assumption of congruent dissolution.

In Fig. 8, three distinct Al environments are observable in each of the cement samples by ^{27}Al MAS NMR spectroscopy. The spectrum of the unreacted slag is observed as a broad hump centred at around 59 ppm representing the distribution of Al sites in the unreacted slag; a contribution from the remnant slag particles is also observed underlying the spectra of the reacted pastes. In the spectra of the pastes, the Al[VI] resonances at chemical shift values below 20 ppm are assigned to the Al sites in the two types of LDH structures (Mg–Al and AFm), and bands at around 60–80 ppm correspond to Al[IV] and are assigned to the tetrahedral Al environments in C–(A)–S–H gel [52,55,58,60].

Significant reductions in the intensities of the broad slag peak centred around 59 ppm, along with an increase in the Al[IV] resonance at 64–80 ppm, take place from 28 to 180 days of curing, which is associated with an increased degree of reaction as the slag continues to be consumed and hydration products form. Unmodified slag pastes with different chemical compositions showed different line shapes between 64–80 ppm, which reflect different Al coordination environments in the C–(A)–S–H gel, the q^2 bridging sites within the higher chemical shift part of this region and the q^3 crosslinking sites at lower chemical shift. Compared with the unmodified samples, the further shift from 59 ppm towards higher chemical shift in 10 wt.% CLDH modified samples represents an increased degree of reaction, corresponding to the analysis presented above.

The peaks centred at 9 ppm in Fig. 8 are attributed to overlapping contributions from the Ca–Al LDH type phases and the hydrotalcite-like phase [36,60], and increased slightly in intensity from 28 to 180 days. Comparing binders produced with different slag sources, the relative intensity of Al[VI] sites compared to Al[IV] sites increased as the MgO content of the slag increased, consistent with the increased formation of LDH phases in the presence of more Mg. Since the slags tested here with higher MgO content also had lower Al_2O_3 content, the total amount of Al incorporated into the C–(A)–S–H gel derived from high

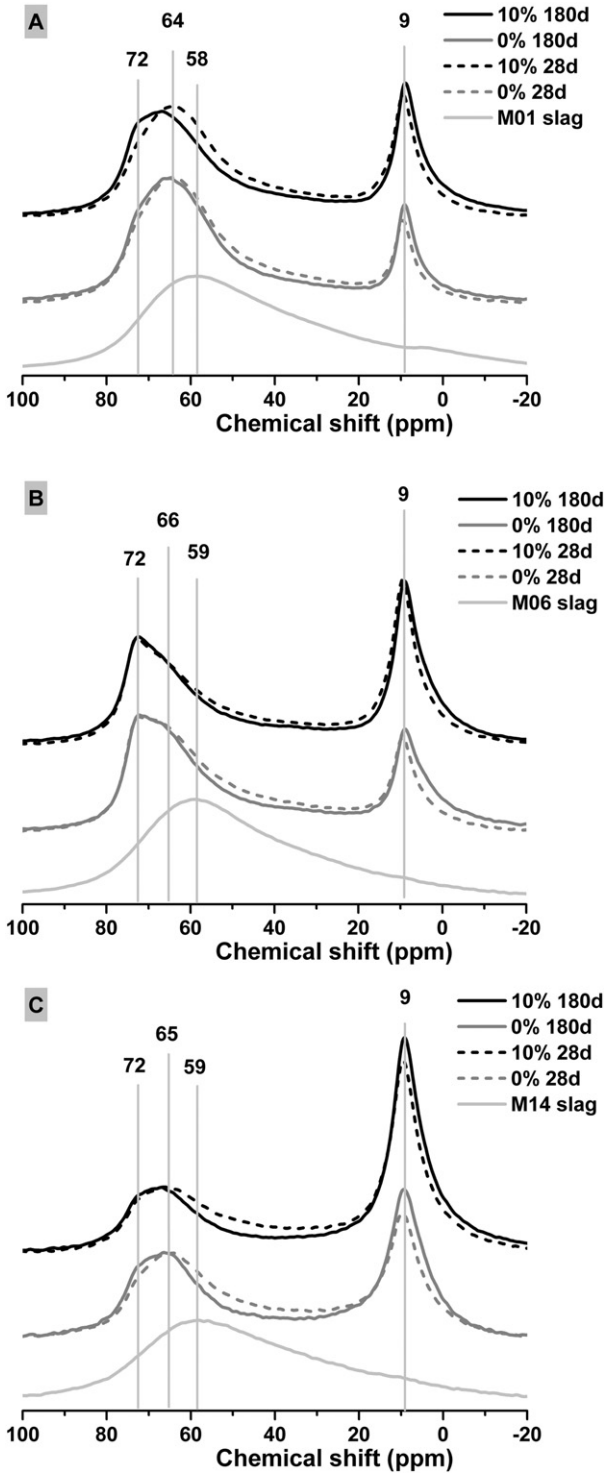

Fig. 8. ^{27}Al MAS NMR spectra of slag pastes prepared using (A) slag M01, (B) slag M06 and (C) slag M14, with 0 wt.% and 10 wt.% of CLDH, cured for 28 and 180 days.

MgO content slag is much lower in low-MgO content slag pastes. This corresponds to the differences in Al/Si ratio calculated in SEM–EDX analysis (Table 5), and the ^{29}Si MAS NMR analysis (Table 6).

The addition of 10 wt.% CLDH led to an increased intensity of the peak assigned to the hydrotalcite-like phase, as a consequence of the recrystallisation of the CLDH to form crystalline Mg–Al LDH. However, as the CLDH addition increased the total aluminium content in the paste, the ^{27}Al MAS NMR spectra do not display a clear trend in the total Al content in the C–(A)–S–H gel before and after CLDH modification.

3.5. The importance of slag chemistry in Na_2CO_3 activated cements

The hardening time of sodium carbonate activated slag pastes is strongly dependent on the slag chemistry. Significantly more rapid kinetics of reaction, and therefore faster setting, have been identified for slags with lower Al_2O_3 but much higher MgO contents, as a consequence of the formation of a high content of LDH phases), consistent with previous studies using sodium silicate as the activator [15–17].

Fig. 9 illustrates a conceptual model which has been developed to describe the importance of the carbonate consumption process in sodium carbonate activation of slag. The black line represents the carbonate route in samples prepared without CLDH addition, while the grey line shows the influence of the CLDH.

Gaylussite is often formed at early age in the sodium carbonate activated paste prior to the formation of C–(A)–S–H [10,12]. This is due to the fact that the breakage of O–Ca bonds and O–Mg bonds to release these species from the slag is able to take place at lower alkalinity than the breakage of O–Al and O–Si bonds [20]. Therefore, the aqueous phase reaches saturation with respect to gaylussite before other phases due to the high activator Na concentration, as shown in Eq. (1). When the LDH phases and C–(A)–S–H gel start to precipitate, the gaylussite dissolves as a result of the decreased CO_3^{2-} ion concentration in the aqueous phase [10], with the carbonate reprecipitating rapidly as $CaCO_3$ polymorphs (e.g. the aragonite observed here) as shown in Eq. (2) [61]. This explains the formation of aragonite in most of the samples here.

$$5H_2O + 2Na^+ + Ca^{2+} + 2CO_3{}^{2-} \rightarrow Na_2Ca(CO_3)_2{\cdot}5H_2O\ (\text{gaylussite}) \quad (1)$$

$$Na_2Ca(CO_3)_2{\cdot}5H_2O \rightarrow CaCO_3(\text{aragonite}) + 2Na^+ + CO_3{}^{2-} + 5H_2O \quad (2)$$

Both the hydrotalcite-like and AFm phases can be stable carbonate-bearing phases in cementitious binders [17,32]. The dissolution of gaylussite would be accelerated if the dissolved CO_3^{2-} ions are taken by the LDH phases and removed from the pore solution. This explains the effect of the slag composition on the rate of reaction, where a higher degree of LDH phase formation accelerates the kinetics of reaction when using a sodium carbonate activator. Upon alkali activation of the slags, LDH phases form as a secondary reaction product, especially the hydrotalcite-like phase, and these phases can act as in-situ carbonate binding agents, promoting the carbonate removal process from the activator to solid phases and consequently accelerating the setting and hardening reaction sequence (Fig. 9).

3.6. Carbonate binding and reaction acceleration by CLDH

The kinetics of reaction of four different slags have all been expedited by the addition of CLDH (Fig. 1), showing that the effectiveness of this addition is not dependent on the type of slag used. The added CLDH will react directly with the activator in aqueous solution, remove carbonate ions from the solution and form hydrotalcite-like phases. This is a shortcut for consumption of carbonate compared with the samples prepared without CLDH, and it also favours the decomposition of gaylussite. However, CLDH does not only act as a carbonate binding agent, as the recrystallisation mechanism of CLDH in an aqueous environment will also modify the chemistry of the system, and this raises the need for further investigation to isolate the exact mechanisms taking place.

The recrystallisation processes of CLDH start with its surface hydroxylation. As the surface oxygen ions of mixed metal oxides are undercoordinated with respect to metal ions, they are highly active in the presence of water and prone to be protonated to hydroxyl groups, as shown in Eq. (3) [62]. When there is sufficient water to react, the mixed metal oxides behave as a Lewis base, forming a conjugate acid ($[Mg_{0.7}Al_{0.3}(OH)_2]^{0.3+}$) and a conjugate base ($OH^-$) as shown in Eq. (4), and the original brucite-like Mg–Al layered structure can

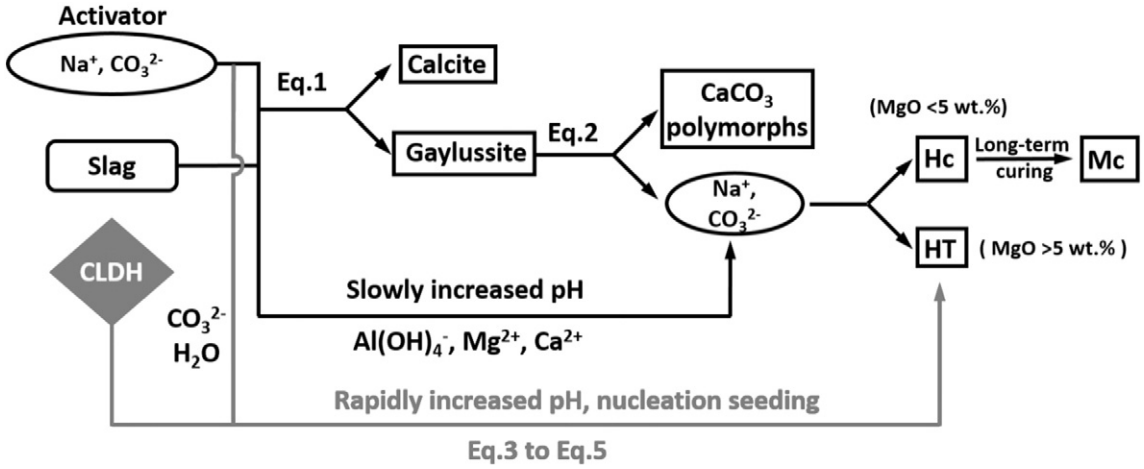

Fig. 9. Simplified schematic diagram of the process of carbonate consumption through binding in mineral carbonates in the absence of CLDH (black), and the extra pathways introduced by CLDH addition, in a Na_2CO_3-activated slag cement.

recrystallise. As a result, the pH of the sodium carbonate solution is increased (see Supporting Information). The sites of conjugate bases are ion-exchangeable with other negatively charged ions [62]. When free CO_3^{2-} ions are available, they will be incorporated into the brucite-like layered structure, forming hydrotalcite as a stable ion-exchanged LDH phase, Eq. (5) [35].

$$\text{-}O^{2-} + H_2O \rightarrow \text{-}OH^- + OH^- \tag{3}$$

$$Mg_{0.7}Al_{0.3}O_{1.15} + 1.15H_2O \rightarrow \left[Mg_{0.7}Al_{0.3}(OH)_2\right]^{0.3+} + 0.3OH^- \tag{4}$$

$$\left[Mg_{0.7}Al_{0.3}(OH)_2\right]^{0.3+} + 0.15\ CO_3^{2-} + nH_2O \rightarrow Mg_{0.7}Al_{0.3}(OH)_2(CO_3)_{0.15} \cdot nH_2O \tag{5}$$

As shown in Eqs. (4) and (5), the recrystallisation processes of the CLDH in sodium carbonate solution produced OH^- and consumed CO_3^{2-} during the initial stage of the reaction (within the first hour), leading to the increase in pH (Supporting Information), which accelerates the reaction.

In addition to this chemical acceleration, the nucleation seeding effects of recrystallised hydrotalcite and the reduced w/b ratio due to the water consumption of CLDH also have the potential to alter the kinetics of reaction. The hydrotalcite-like phase produced by the recrystallisation of CLDH upon reaction with the activator solution (see Supporting Information), is very similar in nature to the Mg–Al LDH which forms as a reaction product in these alkali-activated slag systems, therefore the particle surface of hydrotalcite-like phase could be habitable for precipitation and growing of slag reaction product, including both C–(A)–S–H gel and LDHs. It can be assumed that this would play a similar role in alkali-activated slag systems, acting as a nucleation seed. To investigate the influence of this seeding effect, the sample Ref-1 (Fig. 10) was designed to reflect the seeding effects of the recrystallised hydrotalcite, by replacing CLDH with commercial hydrotalcite. The commercial hydrotalcite is already in its carbonated and hydrated form, and so would not further consume carbonate in the solution or undergo surface hydroxylation.

It is seen from Fig. 10 that the onset time of the acceleration period of sample Ref-1 fell in between that of the plain paste and the 10 wt.% CLDH modified paste. The shift in the acceleration peak towards shorter times demonstrates the seeding effect of the incorporated commercial hydrotalcite, suggesting that the reformed hydrotalcite-like phase which is generated from CLDH upon reaction with the activating solution (see Supporting Information) might also play a similar role in nucleation seeding during the alkali activation process.

However, these effects may also be convoluted by the effects of the change in w/b ratio induced by the uptake of water by the CLDH. Sample Ref-2 (Fig. 10), which has a w/b ratio of 0.35 to correspond to the calculated potential water uptake by the CLDH (Supporting Information) thus aids in isolating any effect of reduced w/b ratio. In the alkali-activated slag system, there might be an optimum w/b ratio at which the hydration kinetics develop faster and the total hydration heat

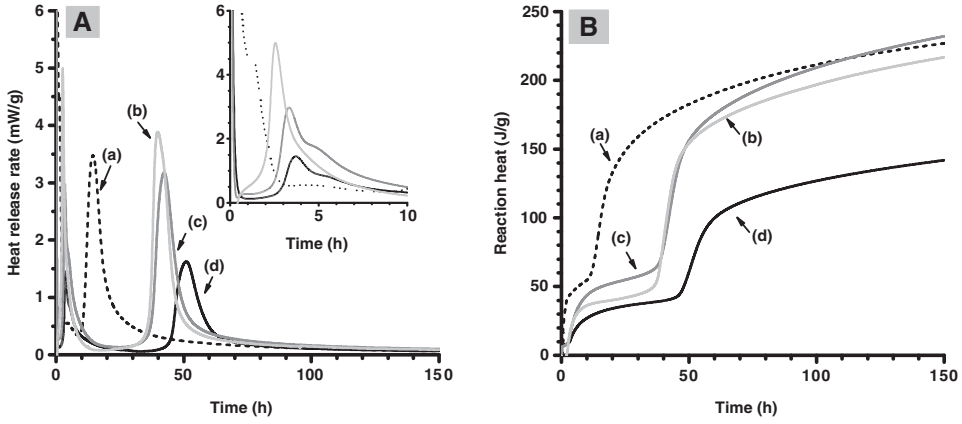

Fig. 10. Isothermal calorimetry data for sodium carbonate activation of slag M06, with (a) a w/b ratio of 0.4, with 10 wt.% CLDH added; (b) a w/b ratio of 0.4 and 10 wt.% commercial hydrotalcite as additives (sample Ref-1); (c) a w/b ratio of 0.35 (sample Ref-2); (d) a w/b ratio of 0.4, without CLDH addition (all the results were normalised by the mass of slag).

release is higher than at any other w/b ratio [63]. For slag M06, w/b = 0.35 appeared to be more closely approaching the optimum w/b ratio than 0.4, which might explain the change of reaction kinetics. However, the workability of the pastes produced at this w/b ratio was more challenging than was the case at the higher w/b ratio used for the other pastes in this study, as the water consumption by the CLDH is gradual and so enables the pastes to be more fluid in the fresh state than is the case for a simple reduction in w/b ratio.

In summary, the incorporation of CLDH expedites the hardening process of sodium carbonate activated slags via several mechanisms, including:

- Increasing the pH of the activator, as observed in the Supporting Information;
- Accelerated consumption of carbonate ions; and
- Hydrotalcite nucleation seeding.

Controlling the reaction kinetics of sodium carbonate-activated slag paste to set within 24 h is desirable for its adoption and implementation by the construction industry. Acceleration of the kinetics of reaction is promoted by expediting the removal of the carbonate supplied by the alkali activator, leaving the slag to react in a NaOH-rich environment [11]. Incorporation of a carbonate binding agent that is more prone than Ca^{2+} to react with the CO_3^{2-} supplied by the sodium carbonate could thus be considered as a feasible approach to accelerate the kinetics of reaction.

4. Conclusions

Control of the kinetics of reaction of sodium carbonate-activated slag has been achieved in this study by adding CLDH as a carbonate binding agent, based on the understanding of the relationship between slag chemistry and the role of the functional group of the activator when producing activated slag cements. The relationships between the various Mg–Al (hydrotalcite-like) and Ca–Al (AFm) layered double hydroxides are essential in determining the overall characteristics of the binder system, as the uptake of Al by these phases restricts its availability for incorporation into C–A–S–H.

In a sodium carbonate-activated binder system, slags containing higher concentrations of MgO are seen to react much more rapidly, and to a greater extent within 180 days of curing. The MgO content of the slag controls the formation of a hydrotalcite-like phase with Mg/Al ~2, and drives the removal of carbonate species from the pore solution. The process of removal of carbonate from the aqueous phase dominates the kinetics of reaction of sodium carbonate activated slag binders. A higher MgO content in the slag leads to faster dissolution and also results in formation of more hydrotalcite, which promotes the consumption of the carbonate species from solution, and accelerates the kinetics of reaction.

Incorporation of up to 10 wt.% CLDH in sodium carbonate activated slag pastes significantly accelerates the kinetics of reaction, enabling the slag pastes to set within 24 h. The incorporated CLDH accelerates the consumption of carbonate, increasing the pH and driving the slag dissolution, and also reduces the effective water/binder ratio through uptake of water as it rehydrates. The hydrotalcite-like phase formed via recrystallisation was dispersed relatively homogeneously in the outer product region of the paste and acted as a nucleation seed, which benefited the precipitation of the gel product.

CLDH addition has therefore been demonstrated to be an effective method by which the sodium carbonate activation of blast furnace slag can be used to produce a cementitious binder with an acceptably fast setting and hardening process for engineering purposes. This is particularly the case when the mix is prepared with a slag containing a high concentration of MgO.

Acknowledgements

This research was funded by the European Research Council under the European Union's Seventh Framework Programme (FP7/2007-2013) / ERC Grant Agreement #335928 (GeopolyConc). Solid-state NMR spectra were obtained at the EPSRC UK National Solid-state NMR Service at Durham. XK thank the China Scholarship Council (CSC) for sponsoring her PhD studies. The technical support provided by Dr. Oday Hussein, and the donation of the slags by ECOCEM® and Prof. Joseé Duchesne (Université Laval, Canada), are also greatly acknowledged.

Appendix A. Supplementary data

Supplementary data to this article can be found online at http://dx.doi.org/10.1016/j.cemconres.2015.11.012.

References

[1] J.S.J. van Deventer, J.L. Provis, P. Duxson, D.G. Brice, Chemical research and climate change as drivers in the commercial adoption of alkali activated materials, Waste Biomass Valoriz. 1 (2010) 145–155.
[2] J.L. Provis, D.G. Brice, A. Buchwald, P. Duxson, E. Kavalerova, P.V. Krivenko, C. Shi, J.S.J. van Deventer, J.A.L.M. Wiercx, Demonstration projects and applications in building and civil infrastructure, in: J.L. Provis, J.S.J. van Deventer (Eds.), Alkali Activated Materials: State-of-the-Art Report, RILEM TC 224-AAM, RILEM/Springer, Dordrecht 2014, pp. 309–338.
[3] J.L. Provis, Geopolymers and other alkali activated materials: why, how, and what? Mater. Struct. 47 (2014) 11–25.
[4] F. Winnefeld, M. Ben Haha, G. Le Saout, M. Costoya, S.-C. Ko, B. Lothenbach, Influence of slag composition on the hydration of alkali-activated slags, J. Sustain. Cem. Based Mater. 4 (2015) 85–100.
[5] S.-D. Wang, K.L. Scrivener, P.L. Pratt, Factors affecting the strength of alkali-activated slag, Cem. Concr. Res. 24 (1994) 1033–1043.
[6] S. Song, D. Sohn, H.M. Jennings, T.O. Mason, Hydration of alkali-activated ground granulated blast furnace slag, J. Mater. Sci. 35 (2000) 249–257.
[7] S.A. Bernal, J.L. Provis, A. Fernández-Jiménez, P.V. Krivenko, E. Kavalerova, M. Palacios, C. Shi, Binder chemistry - High-calcium alkali-activated materials, in: J.L. Provis, J.S.J. van Deventer (Eds.), Alkali-Activated Materials: State-of-the-Art Report, RILEM TC 224-AAM, Springer/RILEM, Dordrecht 2014, pp. 59–91.
[8] J.L. Provis, S.A. Bernal, Geopolymers and related alkali-activated materials, Annu. Rev. Mater. Res. 44 (2014) 299–327.
[9] J.L. Provis, Green concrete or red herring? — future of alkali-activated materials, Adv. Appl. Ceram. 113 (2014) 472–477.
[10] S.A. Bernal, J.L. Provis, R.J. Myers, R. San Nicolas, J.S.J. van Deventer, Role of carbonates in the chemical evolution of sodium carbonate-activated slag binders, Mater. Struct. 48 (2014) 517–529.
[11] S.A. Bernal, R. San Nicolas, J.S.J. van Deventer, J.L. Provis, Alkali-activated slag cements produced with a blended sodium carbonate/silicate activator, Adv. Cem. Res. (2016)http://dx.doi.org/10.1680/adcr.15.00013 (in press).
[12] A. Fernández-Jiménez, F. Puertas, Setting of alkali-activated slag cement. Influence of activator nature, Adv. Cem. Res. 13 (2001) 115–121.
[13] C. Shi, R.L. Day, Some factors affecting early hydration of alkali-slag cements, Cem. Concr. Res. 26 (1996) 439–447.
[14] A. Fernández-Jiménez, F. Puertas, Effect of activator mix on the hydration and strength behaviour of alkali-activated slag cements, Adv. Cem. Res. 15 (2003) 129–136.
[15] M. Ben Haha, B. Lothenbach, G. Le Saout, F. Winnefeld, Influence of slag chemistry on the hydration of alkali-activated blast-furnace slag — part II: effect of Al_2O_3, Cem. Concr. Res. 42 (2012) 74–83.
[16] M. Ben Haha, B. Lothenbach, G. Le Saout, F. Winnefeld, Influence of slag chemistry on the hydration of alkali-activated blast-furnace slag — part I: effect of MgO, Cem. Concr. Res. 41 (2011) 955–963.
[17] S.A. Bernal, R. San Nicolas, R.J. Myers, R. Mejía de Gutiérrez, F. Puertas, J.S.J. van Deventer, J.L. Provis, MgO content of slag controls phase evolution and structural changes induced by accelerated carbonation in alkali-activated binders, Cem. Concr. Res. 57 (2014) 33–43.
[18] A.R. Sakulich, E. Anderson, C.L. Schauer, M.W. Barsoum, Influence of Si:Al ratio on the microstructural and mechanical properties of a fine-limestone aggregate alkali-activated slag concrete, Mater. Struct. 43 (2010) 1025–1035.
[19] A.R. Sakulich, E. Anderson, C. Schauer, M.W. Barsoum, Mechanical and microstructural characterization of an alkali-activated slag/limestone fine aggregate concrete, Constr. Build. Mater. 23 (2009) 2951–2957.
[20] C. Shi, R.L. Day, A calorimetric study of early hydration of alkali-slag cements, Cem. Concr. Res. 25 (1995) 1333–1346.
[21] S. Miyata, The syntheses of hydrotalcite-like compounds and their structures and physico-chemical properties I: the systems Mg^{2+}–Al^{3+}–NO_3^-, Mg^{2+}–Al^{3+}–Cl^-, Mg^{2+}–Al^{3+}–ClO_4^-, Ni^{2+}–Al^{3+}–Cl^- and Zn^{2+}–Al^{3+}–Cl^-, Clay Clay Miner. 23 (1975) 369–375.
[22] S.J. Mills, A.G. Christy, J.-M.R. Genin, T. Kameda, F. Colombo, Nomenclature of the hydrotalcite supergroup: natural layered double hydroxides, Mineral. Mag. 76 (2012) 1289–1336.

[23] M.C.D. Mourad, M. Mokhtar, M.G. Tucker, E.R. Barney, R.I. Smith, A.O. Alyoubi, S.N. Basahel, M.S.P. Shaffer, N.T. Skipper, Activation and local structural stability during the thermal decomposition of Mg/Al-hydrotalcite by total neutron scattering, J. Mater. Chem. 21 (2011) 15479–15485.
[24] T. Hibino, Y. Yamashita, K. Kosuge, A. Tsunashima, Decarbonation behavior of Mg–Al–CO_3 hydrotalcite-like compounds during heat treatment, Clay Clay Miner. 43 (1995) 427–432.
[25] L. Lv, J. He, M. Wei, D.G. Evans, X. Duan, Uptake of chloride ion from aqueous solution by calcined layered double hydroxides: equilibrium and kinetic studies, Water Res. 40 (2006) 735–743.
[26] L. Lv, J. He, M. Wei, X. Duan, Kinetic studies on fluoride removal by calcined layered double hydroxides, Ind. Eng. Chem. Res. 45 (2006) 8623–8628.
[27] M. León, E. Díaz, S. Ordóñez, Ethanol catalytic condensation over Mg–Al mixed oxides derived from hydrotalcites, Catal. Today 164 (2011) 436–442.
[28] D. Tichit, M. Naciri Bennani, F. Figueras, R. Tessier, J. Kervennal, Aldol condensation of acetone over layered double hydroxides of the meixnerite type, Appl. Clay Sci. 13 (1998) 401–415.
[29] Z. Yang, H. Fischer, R. Polder, Synthesis and characterization of modified hydrotalcites and their ion exchange characteristics in chloride-rich simulated concrete pore solution, Cem. Concr. Compos. 47 (2014) 87–93.
[30] S. Yoon, J. Moon, S. Bae, X. Duan, E.P. Giannelis, P.M. Monteiro, Chloride adsorption by calcined layered double hydroxides in hardened portland cement paste, Mater. Chem. Phys. 145 (2014) 376–386.
[31] E. Kanezaki, Thermal behavior of the hydrotalcite-like layered structure of Mg and Al-layered double hydroxides with interlayer carbonate by means of in situ powder HTXRD and DTA/TG, Solid State Ionics 106 (1998) 279–284.
[32] T. Matschei, B. Lothenbach, F.P. Glasser, The AFm phase in Portland cement, Cem. Concr. Res. 37 (2007) 118–130.
[33] M. Whittaker, M. Zajac, M. Ben Haha, F. Bullerjahn, L. Black, The role of the alumina content of slag, plus the presence of additional sulfate on the hydration and microstructure of Portland cement-slag blends, Cem. Concr. Res. 66 (2014) 91–101.
[34] G. Mascolo, M.C. Mascolo, On the synthesis of layered double hydroxides (LDHs) by reconstruction method based on the "memory effect", Microporous Mesoporous Mater. 214 (2015) 246–248.
[35] K. Morimoto, S. Anraku, J. Hoshino, T. Yoneda, T. Sato, Surface complexation reactions of inorganic anions on hydrotalcite-like compounds, J. Colloid Interface Sci. 384 (2012) 99–104.
[36] J. Rocha, M. del Arco, V. Rives, M.A. Ulibarri, Reconstruction of layered double hydroxides from calcined precursors: a powder XRD and ^{27}Al MAS NMR study, J. Mater. Chem. 9 (1999) 2499–2503.
[37] A. Ipavec, R. Gabrovšek, T. Vuk, V. Kaučič, J. Maček, A. Meden, Carboaluminate phases formation during the hydration of calcite-containing portland cement, J. Am. Ceram. Soc. 94 (2011) 1238–1242.
[38] D. Damidot, S. Stronach, A. Kindness, M. Atkins, F.P. Glasser, Thermodynamic investigation of the $CaO–Al_2O_3–CaCO_3–H_2O$ closed system at 25 °C and the influence of Na_2O, Cem. Concr. Res. 24 (1994) 563–572.
[39] T. Matschei, B. Lothenbach, F.P. Glasser, Thermodynamic properties of Portland cement hydrates in the system $CaO–Al_2O_3–SiO_2–CaSO_4–CaCO_3–H_2O$, Cem. Concr. Res. 37 (2007) 1379–1410.
[40] S.-D. Wang, K.L. Scrivener, Hydration products of alkali activated slag cement, Cem. Concr. Res. 25 (1995) 561–571.
[41] J.I. Escalante-García, A.F. Fuentes, A. Gorokhovsky, P.E. Fraire-Luna, G. Mendoza-Suarez, Hydration products and reactivity of blast-furnace slag activated by various alkalis, J. Am. Ceram. Soc. 86 (2003) 2148–2153.
[42] R.J. Myers, E. L'Hôpital, J.L. Provis, B. Lothenbach, Effect of temperature and aluminium on calcium (alumino)silicate hydrate chemistry under equilibrium conditions, Cem. Concr. Res. 68 (2015) 83–93.
[43] R. Fischer, H.J. Kuzel, Reinvestigation of the system $C_4A.nH_2O–C_4A.CO_2.nH_2O$, Cem. Concr. Res. 12 (1982) 517–526.
[44] B. Lothenbach, G. Le Saout, E. Gallucci, K. Scrivener, Influence of limestone on the hydration of Portland cements, Cem. Concr. Res. 38 (2008) 848–860.
[45] R.J. Myers, B. Lothenbach, S.A. Bernal, J.L. Provis, Thermodynamic modelling of alkali-activated slag cements, Appl. Geochem. 61 (2015) 233–247.
[46] F.P. Glasser, A. Kindness, S.A. Stronach, Stability and solubility relationships in AFm phases: part I. Chloride, sulfate and hydroxide, Cem. Concr. Res. 29 (1999) 861–866.
[47] M.C. Gastuche, G. Brown, M.M. Mortland, Mixed magnesium–aluminium hydroxides i. Preparation and characterization of compounds formed in dialysed systems, Clay Miner. 7 (1967) 177–192.
[48] X. Duan, D.G. Evans (Eds.), Layered Double Hydroxides, Springer, Berlin Heidelberg, 2006.
[49] R. San Nicolas, S.A. Bernal, R. Mejía de Gutiérrez, J.S.J. van Deventer, J.L. Provis, Distinctive microstructural features of aged sodium silicate-activated slag concretes, Cem. Concr. Res. 65 (2014) 41–51.
[50] C. Famy, K.L. Scrivener, A.K. Crumbie, What causes differences of C–S–H gel grey levels in backscattered electron images? Cem. Concr. Res. 32 (2002) 1465–1471.
[51] E. L'Hôpital, B. Lothenbach, G. Le Saout, D. Kulik, K. Scrivener, Incorporation of aluminium in calcium–silicate–hydrates, Cem. Concr. Res. 75 (2015) 91–103.
[52] R.J. Myers, S.A. Bernal, J.D. Gehman, J.S.J. van Deventer, J.L. Provis, The role of Al in cross-linking of alkali-activated slag cements, J. Am. Ceram. Soc. 98 (2014) 996–1004.
[53] R. Snellings, Surface chemistry of calcium aluminosilicate glasses, J. Am. Ceram. Soc. 98 (2015) 303–314.
[54] R.J. Kirkpatrick, MAS NMR-spectroscopy of minerals and glasses, Rev. Mineral. 18 (1988) 341–403.
[55] S.-D. Wang, K.L. Scrivener, ^{29}Si and ^{27}Al NMR study of alkali-activated slag, Cem. Concr. Res. 33 (2003) 769–774.
[56] I.G. Richardson, A.R. Brough, R. Brydson, G.W. Groves, C.M. Dobson, Location of aluminum in substituted calcium silicate hydrate (C–S–H) gels as determined by ^{29}Si and ^{27}Al NMR and EELS, J. Am. Ceram. Soc. 76 (1993) 2285–2288.
[57] J. Schneider, M.A. Cincotto, H. Panepucci, ^{29}Si and ^{27}Al high-resolution NMR characterization of calcium silicate hydrate phases in activated blast-furnace slag pastes, Cem. Concr. Res. 31 (2001) 993–1001.
[58] G. Engelhardt, D. Michel, High Resolution Solid State NMR of Silicates and Zeolites, John Wiley & Sons, Chichester, 1987.
[59] R.J. Myers, S.A. Bernal, R. San Nicolas, J.L. Provis, Generalized structural description of calcium–sodium aluminosilicate hydrate gels: the cross-linked substituted tobermorite model, Langmuir 29 (2013) 5294–5306.
[60] M.R. Jones, D.E. Macphee, J.A. Chudek, G. Hunter, R. Lannegrand, R. Talero, S.N. Scrimgeour, Studies using ^{27}Al MAS NMR of AFm and AFt phases and the formation of Friedel's salt, Cem. Concr. Res. 33 (2003) 177–182.
[61] J.L. Bischoff, D.B. Herbst, R.J. Rosenbauer, Gaylussite formation at Mono Lake, California, Geochim. Cosmochim. Acta 55 (1991) 1743–1747.
[62] H. Tamura, K. Mita, A. Tanaka, M. Ito, Mechanism of hydroxylation of metal oxide surfaces, J. Colloid Interface Sci. 243 (2001) 202–207.
[63] S.A. Bernal, R. San Nicolas, J.S.J. van Deventer, J.L. Provis, Water content modifies the structural development of sodium metasilicate-activated slag binders, ALCONPAT J. 5 (2015) 29–40.